Sensors & Actuators: B. Chemical 427 (2025) 137194

Contents lists available at ScienceDirect

Sensors and Actuators: B. Chemical

journal homepage: www.elsevier.com/locate/snb

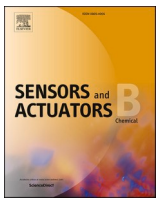

Multivariate sensing of ions using machine learning and composite 2D-3D graphene oxide-hexacyanoferrate electrodes

Laura Malavolta [a], Ilenia Bracaglia [a], Giulia Cazzador [b], Alessandro Kovtun [a], Lorenzo Tomasi [a], Chiara Zanardi [a,b,*], Vincenzo Palermo [a,c,*]

[a] Institute for Organic Synthesis and Photoreactivity, National Research Council (ISOF-CNR), Via P. Gobetti 101, Bologna 40129, Italy
[b] Department of Molecular Sciences and Nanosystems, Ca' Foscari University of Venice, Via Torino 155, Venezia-Mestre 30172, Italy
[c] Department of Industrial and Materials Science, Chalmers University of Technology, Gothenburg S-41296, Sweden

ARTICLE INFO

Keywords:
Artificial intelligence
Graphene oxide
Prussian blue
Nickel hexacyanoferrate
Metal ion detection

ABSTRACT

The conventional method for sensing relies on the development of highly selective materials capable of detecting specific target molecules or ions without interference from other species commonly found in real solutions. However, creating practical sensors that can effectively discriminate between analytes sharing similar chemistry presents significant challenges. To address this issue, we describe a novel approach utilizing an ensemble of four diverse amperometric sensors obtained for deposition of 2-dimensional graphene oxide nanosheets (GO) and 3-dimensional metal-organic frameworks (MOFs) based on redox active metal hexacyanoferrates. The multivariate signals obtained by the sensor array is used to train an artificial neural network (ANN) capable of analysing such complex inputs to accurately determine the concentrations of Na^+ and K^+ ions in solutions with varying ionic strengths. The sensing strategy is based on the differential intercalation and diffusion behaviour of Na^+ and K^+ ions within both GO and MOFs, resulting in distinct voltammetric signals. The neural network is trained using massive datasets comprising 327 variables as columns and over 4 million samples as rows. Following training, the sensor array demonstrates remarkable proficiency in accurately measuring the concentration of both ions present in solution, while a single sensor cannot discern between the signals generated by each ion. This ongoing work underscores the potential of integrating artificial intelligence with tunable materials to develop a new class of chemical sensors with enhanced discrimination capabilities, paving the way for more robust and versatile sensor technologies.

1. Introduction

Biofluids like sweat, tears, and saliva are a challenging matrix to analyze, since they contain a variable combination of inorganic ions, small molecules, large biomolecules and polymers [1–11]. For this reason, the continuous monitoring of health indicators in biofluids is often a demanding task. The approach normally followed is to use one highly selective sensor for each analyte to be detected (Fig. 1a). As example, multisensory platforms have been proposed for the continuous monitoring of important electrolytes such as Na^+ and K^+ [12].

In last years, the development of powerful techniques based on artificial intelligence (AI) and Deep Learning (DL) enabled to analyze large amounts of data to extract useful information from them even in absence of linear and perfectly classified inputs. In particular, artificial neural networks (ANN) mimic the learning process of a simple brain by processing raw data through a network of nodes connected with each other (Fig. 1b). The connections between each node are adjusted through a "training" or "learning" process, where the network is fed with the raw data, while providing the correct final answers. At each iteration, the network evolves "learning" to improve its answers and to match each set of data with the correct answer. Eventually, if the learning process is effective, the algorithm will be able to analyze unknown data, providing the correct answer.

In this work we describe the use of ANN to analyze a large amount of data coming from a sensor array and to quantify the concentration of the two different ions. At difference from selective sensors, the goal here is to demonstrate that a meaningful and robust analysis can be obtained with sensors which are not highly selective. To demonstrate such concept, we chose a significant couple of test analytes, namely Na^+ and K^+ ions.

* Corresponding authors at: Institute for Organic Synthesis and Photoreactivity, National Research Council (ISOF-CNR), Via P. Gobetti 101, Bologna 40129, Italy.
E-mail addresses: chiara.zanardi@unive.it (C. Zanardi), vincenzo.palermo@isof.cnr.it (V. Palermo).

https://doi.org/10.1016/j.snb.2024.137194
Received 9 September 2024; Received in revised form 24 December 2024; Accepted 25 December 2024
Available online 26 December 2024

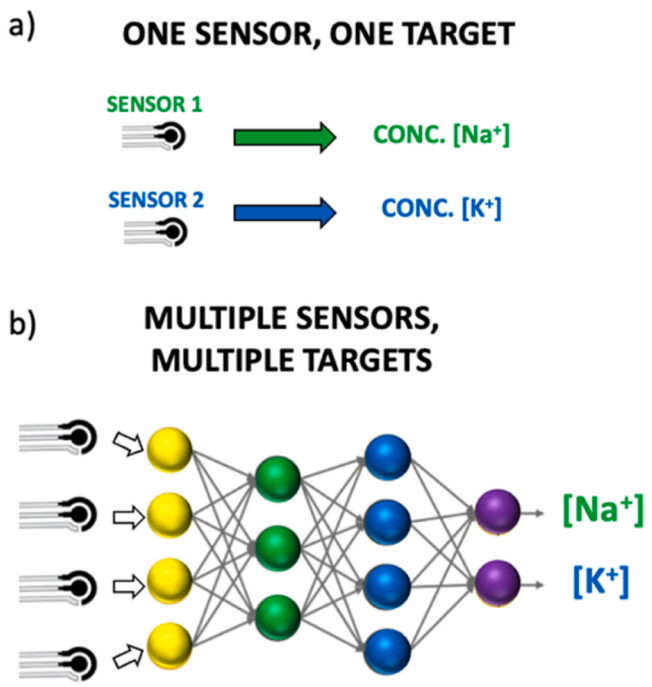

Fig. 1. Schematic representation of ANN architecture applied to electrochemical sensors.

The quantification of Na^+ and K^+ is quite important to define the physiological state of individuals, especially concerning the hydration state. These electrolytes are present in relevant quantities in biological fluids and for this reason their presence significantly affects the ionic strength of the matrix.

The quantification of these ions is generally performed by ion-selective electrodes [13]. The main drawback of these systems is that their response (i.e. the potential) is linearly dependent on the logarithm of the concentration of the analyte and that, for thermodynamic reasons, this dependence is characterized by a Nernstian slope, i.e. 0.059 V per logarithmic unit of either Na^+ or K^+ concentration. This implies that the sensitivity is rather poor and cannot be improved [14,15]. Conversely, amperometric sensing would be advantageous since the signal, i.e. the current intensity, is linearly proportional to the concentration of the analyte in solution [16] and the sensitivity can be modulated by suitable modification of the electrode surface. However, the detection of electrolytes such as Na^+ and K^+ by this unconventional approach is not trivial, since these species are not electroactive.

To this aim, we used, as sensors, electrodes obtained for deposition of a combination of 3-dimensional metal-organic frameworks (MOF) and 2D materials (Fig. 2a-d).

Iron hexacyanoferrate, also known as Prussian blue (PB), is a well known MOF. It is a face-centered cubic (FCC) inorganic salt containing Fe^{3+} positive sites and $Fe(CN)_6^{4-}$ negative ones (Fig. 2e); it is generally described with the chemical formula $Fe_4^{III}[Fe^{II}(CN)_6]_3{\cdot}xH_2O$, although some Fe^{3+} centers are normally replaced by alkaline ions, typically K^+. The cubic unit cell possesses a dimension of 10.2 Å and channels with a diameter of about 3.2 Å, which allow the selective diffusion of species possessing a low molecular weight, such as water molecules, which normally fill the resultant unit cell of PB. This material behaves as a receptor of alkali cations within its crystalline structure during the redox processes involving the Fe^{3+}/Fe^{2+} centers occurring in the region close to 0 V *vs.* Ag/AgCl reference electrode [17–20], which is described by reaction [21]:

$$A_{z-y}Fe_y^{III}[Fe^{II}(CN)_6]_2 + yA^+ + ye^- \rightleftarrows A_zFe_y^{II}[Fe^{II}(CN)_6]_2 \quad (1)$$

Due to the dimension of the channels, the access of A^+ ions can be more or less hindered depending on the dimension of the hydrated ions, so that the shape of the voltammetric response results, in turn, influenced. Since K^+ ions (hydrated radius $r = 3$ Å) can easily penetrate the crystalline structure of PB, the Fe^{3+}/Fe^{2+} reduction process is evidenced by a very sharp reversible peak. On the contrary, due to the larger dimension of Na^+ ions (hydrated radius $r = 4$ Å), the peak results broader and shifted to more negative potential values.

If Fe^{3+} ions of PB are replaced with different heavy metals, we shall obtain a MOF with similar lattice of PB but with different electrochemical properties. In particular, when Fe^{III} is replaced by Ni^{II} we obtain Nickel Hexacyanoferrate (termed NH) which can undergo the exchange of A^+ in the crystalline structure in the process involving the reversible oxidation of $[Fe(CN)_6]^{4-}$ centers, described by reaction (2):

$$[A_{1+y}Ni^{2+}Fe^{II}(CN)_6] \rightleftarrows [ANi^{2+}Fe^{III}(CN)_6] + yA^+ + ye^- \quad (2)$$

Also in this case the dimension of the hydrated ion may affect the shape of the redox process, so that the oxidation of NH in solutions containing K^+ ions results in a double peak, at difference with a similar process recorded in solutions only containing Na^+ [22].

Due to this peculiar behavior, hexacyanoferrates have already been proposed for the quantification of K^+ on the basis of the peak potential at which the voltammetric processes occur [21,23–25]. However, this conventional univariate approach shows poor accuracy for the quantification of Na^+ and K^+ mixtures in more complex matrices.

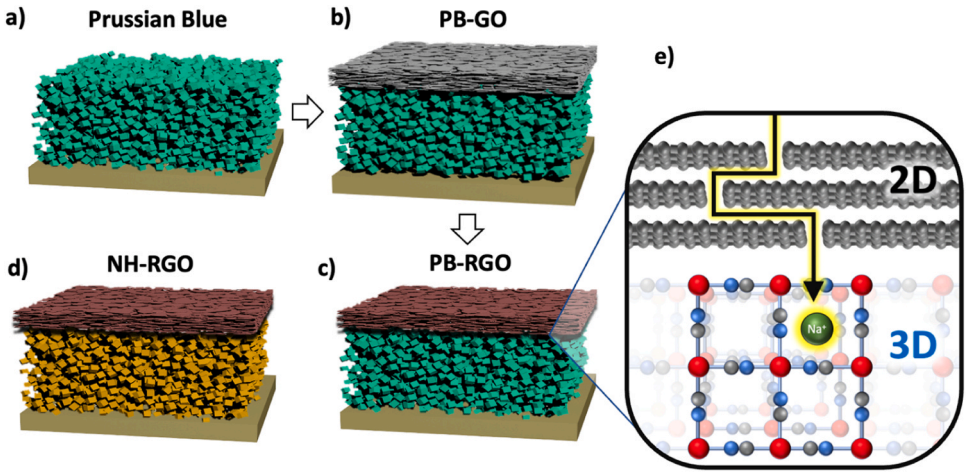

Fig. 2. (a-d) Schematic representations of the electrode coatings used in the sensor platform for the selective quantification of Na^+ and K^+ by ANN. (e) Cartoon showing the diffusion and intercalation of Na ions in PB-RGO electrodes.

Table 1
Composition of the solutions used to train the algorithm.

Solution n.	1	2	3	4	5	6	7	8	9	10	11	12
Na^+ (M)	0	0	10^{-4}	10^{-4}	10^{-4}	10^{-3}	10^{-3}	10^{-3}	10^{-2}	10^{-2}	10^{-1}	10^{-1}
K^+ (M)	10^{-4}	10^{-3}	0	10^{-4}	10^{-3}	0	10^{-4}	10^{-3}	10^{-5}	10^{-2}	10^{-5}	10^{-2}
NH_4^+ (M)	10^{-1}											

An alternative method, already exploited in similar cases [26,27], tries to extract quantitative information from the whole voltammetric trace using a multivariate approach and combining information deriving from different sensors. We thus used here an array of four electrochemical sensors, two containing PB and two NH as the sensing element for the amperometric simultaneous detection of Na^+ and K^+ in aqueous solutions. The amperometric detection also takes advantage of the deposition of Graphene Oxide (GO), then electrochemically reduced to electrically conductive reduced graphene oxide (RGO, Fig. 2) to further improve selectivity.

Thanks to the 2-dimensional structure, also GO is an ideal material for selective ion sieving: ions and molecules will diffuse in stacked GO multilayers in tortuous paths [28]. In a recent work [29], we demonstrated that monovalent ions like Na^+ and K^+ can be transported through GO by applying a low electric voltage, while divalent ions are blocked, with K^+ diffusing faster than Na^+. The diffusion was influenced not only by steric factors (e.g. the hydrated radius *r*) but also by chemical ones, with ions interacting significantly with the charged groups present on GO. Indeed, GO and RGO are often applied in electrochemical sensing, thanks to their known unique properties, such as the high mechanical stability, the large surface area, and the easy surface functionalization [30–34].

Thus, we prepared screen printed electrodes (SPEs) modified with either PB or NH at two different thickness each, then coated by electrochemically reduced GO to form PB-RGO and NH-RGO, respectively. All combined, they form the 4-electrode platform used to test solutions at various Na^+ and K^+ concentration. The accuracy of the detection was ensured with the combination of voltammetric signals deriving from the four sensors types, then fed to an algorithm trained using a DL approach [35].

In detail, we used a feed-forward ANN [36] which was trained experimentally by collecting sensors signals in solutions with well-defined, known composition. This allowed the prediction of one or more required outputs, namely the concentration of target species as alkali ions [37], in an unknown solution, hopefully achieving a high level of accuracy (Fig. 1b) [38]. The process passes through the hidden layers that elaborate the data using internal parameters as “weights” [35,38]. The activation function considered, which transforms each output node of a former layer into the input of the following one, is the Rectified Linear Unit (ReLU) [39,40]. At each iteration of the algorithm [41] the system calculates an error between predicted and true output values (termed “loss function”) to provide feedback to the algorithm (backward propagation); in this way, internal weights are adjusted and then applied to each node of the network, according to the matrix of interconnections [35]. The process is repeated for many training cycles, also termed “epochs”. This forward and backward loop continues until the error is minimized and the final weights are thus calculated [42].

The voltammetric data produced by multiple copies of the four elements of the electrochemical platform and collected in solutions of Na^+ and K^+ at variable molar ratio were divided between training set and test set. The training set was used to define the prediction model by DL data elaboration, then the test set was used to verify the ability of the trained models to predict the concentration of the two electrolytes in solution.

2. Materials and methods

2.1. Materials and instruments

Potassium chloride, sodium chloride, hydrochloric acid, nickel(II) chloride hexahydrate, acetic acid, sodium acetate and potassium acetate were purchased from Sigma Aldrich. Potassium hexacyanoferrate(III), and iron(III) chloride hexahydrate were purchased from Carl Roth. Ammonium chloride was purchased from Carlo Erba Reagents srl. GO powder (<35 mesh, >90 % of the sheets with lateral size 300–3000 nm) was purchased from LayerOne and suspended in ultrapure water (18 MΩ·cm resistivity) to achieve a final 1 mg/mL dispersion.

Electrochemical deposition and measurements of the coatings were done with a μStat400 bi-potentiostat/galvanostat and a μStat8000 multi-potentiostat/galvanostat, both purchased from Dropsens-Metrohm. All the measurements were carried out starting with carbon-based SPEs. Preliminary tests were carried out by DS110 electrode platforms possessing a 4 mm diameter working electrode, whereas the measurements aimed at defining the prediction algorithm were obtained by an array of 96 different SPE, containing 3 mm diameter working electrodes, driven by a commercial connector 96 × module (Dropsens-Metrohm) working in combination with the multichannel potentiostat.

2.2. Sensor fabrication

PB-RGO electrodes were obtained starting from the galvanostatic deposition of a PB film [34,43] performed at −40 μA cm^{-2} for either 60 or 120 s from a solution containing 2 mM $K_3[Fe(CN)_6]$, 2 mM $FeCl_3$, 0.1 M KCl, and 10 mM HCl. In these conditions, ferricyanide is reduced to ferrocyanide, with subsequent precipitation of PB. The electrodes were then rinsed with a 10 mM HCl solution and hereafter called as PB_{60} and PB_{120}, respectively. Then, GO was drop cast from water solutions on the electrodes and electrochemically transformed in RGO by applying a constant voltage of −1.25 V for 180 s in a 0.1 M phosphate buffer solution (pH 7) containing 0.1 M KCl, to obtain the final PB_{60}-RGO and PB_{120}-RGO electrodes, respectively.

NH-RGO surfaces were obtained in similar way, but starting from the electrochemical deposition of NH, performed by dropping a precursor solution containing 1.2 mM $NiCl_2 \bullet 6\,H_2O$, 0.5 mM $K_3[Fe(CN)_6]$, and 0.05 M KCl on the 3-electrode cell of the electrode. The working electrode was polarized between −0.1 and 1 V, in either 20 or 50 voltammetric cycles at 20 mVs^{-1} scan rate, to obtain NH_{20} and NH_{50}, respectively. The electrode was then rinsed with distilled water and 20 μL cm^{-2} of a 1 mg/mL GO dispersion was drop cast onto the surface before being electrochemically reduced as described before. These electrodes will be hereafter called NH_{20}-RGO and NH_{50}-RGO, respectively.

Table 2
Dataset structure built for the training of PB_{60}-RGO, PB_{120}-RGO, NH_{20}-RGO, NH_{50}-RGO, sensors.

SENSORS INPUT				ADDITIONAL INPUT		
PB_{60}-RGO	PB_{120}-RGO	NH_{20}-RGO	NH_{50}-RGO	Analyte 1 concentration	Analyte 2 concentration	Cycle Number
A_1,. A_{81}	A_1,. A_{81}	A_1,. A_{81}	A_1,. A_{81}	[Na^+]	[K^+]	C_1,… C_{69}

2.3. Cyclic voltammetry in K^+/Na^+ solutions

First, we verified the capability of PB and NH coatings to discriminate solutions containing different amounts of K^+ and Na^+ at a fixed ionic strength of 0.1 M. To this aim, we prepared five solutions of acetate buffer (0.1 M, pH 4.8) at varying the concentration of the two ions from 0 to 0.1 M to obtain different K^+/Na^+ ratio (100:0; 75:25; 50:50; 25:75; 0:100). CV responses were collected from +0.5 to −0.3 V and from +00.8–0.0 V at electrodes containing PB or NH, respectively; the scan rate was 0.02 Vs^{-1} in all tests.

Additional CV measurements were carried out adding an interfering ion (NH_4Cl, 0.1 M) to the previous solutions, to test the electrodes in realistic solutions, more similar to the composition of the human sweat.

2.4. Data collection with the 4-electrode platform

Multiple copies of the 4-electrode types PB_{60}-RGO, PB_{120}-RGO, NH_{20}-RGO, and NH_{50}-RGO were obtained by functionalization of 96 ×SPE plates. To record at least 1000 curves in each solution for each kind of electrode, we used five plates replicating 120 times the 4-electrode array. The composition of the various solutions tested in this case is reported in Table 1; they are chosen to possess a fixed concentration of NH_4Cl and a concentration of K^+ varying from 0 to 0.01 M, and and a concentration of Na^+ varying from 0 M to 0.1 M, respectively mimicking the concentrations normally present in sweat. In all solutions, the concentration of interfering species NH_4^+ was orders of magnitude larger or at best equal to the concentration of the target analytes.

Each solution was analyzed with multiple electrodes obtained in similar conditions, collecting 70 CV responses each time. For these analyses, we decided to restrict the potential window for the acquisition of the CV responses as compared to the initial tests described in Section 2.3, to shorten the time required for recording all the responses required to train the algorithm. To such a purpose, the potential was cycled between +0.6 and +0.2 V for NH-RGO electrodes and from +0.3 V to −0.1 V for PB-RGO electrodes.

2.5. Dataset structure

CV data were stored in comma separated values (CSV) files, each one containing 161 points representing couples of potential and current values. In total, we collected more than 29000 CSV files of valid data. We split each CV curve into two different sections of the dataframe, acquired during the forward and backward ramp of the cycle, respectively. Thus, each curve, consisting of 161 data points, was split into two sets of 81 data points each termed A_1, A_2,. A_{81}. The middle point (i.e. the one at the lowest extreme potential of the scanned potential range) was duplicated in both sets.

Data were aquired in parallel from various devices for every type of sensor. A main issue of electrochemical sensors is their stability, i.e. changes in response with time. That's why we included also the cycle number (C_1, C_2, corresponding to the "age" of the sensor) as an input of the algorithm. Each sensor performed a sequence of 70 cycles in each solution; the values from the first voltammetric cycle (C_0) was discarded to avoid any artefact due to possible pollution coming from previous experiments. This means that we considered the current values collected in the following cycles labelled C_1…C_{69} for the construction of the algorithm. Each line of the dataset included as further variables the set concentration of Na^+ and K^+ of the relevant solutions. Table 2 shows the structure of a typical dataframe used.

During the data pre-processing we also operated a cartesian product of the acquisitions for each cycle and for each solution to significantly increase the dimension of the dataset. In other words, we assumed that each acquisition deriving from a single sensor was a possible acquisition by a sensor of that type. Thus, considering the different types of sensors, each combination among their responses was a possible real acquisition from a 4-electrode platform. This approach finally led to two dataframes with 327 variables as columns (4 ×81 current data + cycle number + Na^+ conc. + K^+ conc., see Table 2) and > 4 million samples as rows.

3. Results and discussion

3.1. Characterization of electrode coatings

We first verified the capability of bare PB sensors to discriminate among solutions containing different amount of K^+ and Na^+, despite a fixed ionic strength. To this aim, we prepared five solutions at different K^+/Na^+ ratio and we collected CV responses from +0.5 to −0.3 V. We obtained responses characterized by a shape strongly dependent on the composition of the solution (Fig. S1a in ESI). As expected, when only K^+ was present in solution, the voltammogram was characterized by a sharp reduction peak centered at 0.06 V, whereas a broad reduction peak centered at −0.06 V was recorded in solutions only containing Na^+. In solutions containing a mixture of Na^+ and K^+ we observed intermediate situations with variations in both the peak potential and the shape of the response. The shift of the reduction peak to less negative potential with increasing concentration of K^+ in solution can be explained by considering that this ion can more easily penetrate the structure of PB since its hydrated radius is smaller than that of Na^+ [19,23]. Unfortunately, the stability of the PB deposit depends on the presence of K^+ in solution: in agreement to what reported in literature [19], this ion can be intercalated inside the PB crystal structure enhancing the stability of the coating.

Thus, to improve the stability of the sensing element, a thin coating of GO was drop cast and reduced on the PB deposit. The use of GO and RGO to stabilize unstable active materials on electrodes has been extensively demonstrated in past works, in particular for electrodes for energy storage [44].

SEM images collected at different magnification (Figs. S2–4c in ESI) confirmed that GO formed a homogeneous film completely covering the nanosized structure of the MOF. The image collected in cross section (Fig. S5c) showed that the GO coating was very thin (<1 μm). The presence of the GO coating did not alter the voltammetric behavior of the metal complex in presence of the Na^+/K^+ mixture with respect to that observed for pristine PB (Fig. S1bin ESI), but improved the stability of the coating especially when the concentration of K^+ was low, as often happens in sweat samples. CV curves obtained in this case still varied with Na^+/K^+ ratio, but the intensities of the current recorded were lower, likely due to the presence of an additional nanometric barrier of a poorly conductive material. Faradic currents registered at PB_{60}-GO were anyhow higher than those expected for the presence of an insulating coating, since GO is permeable to alkaline ions [29].

The external GO coating could be easily reduced to RGO by thermal, chemical or electrochemical method increasing the electrical conductivity of the material [45]. The electrochemical approach was the most spontaneous choice for this specific application [46]. SEM images collected for the resulting PB_{60}-RGO confirmed that the coating maintained its homogeneous continuous structure even after reduction (Figs. S2–4d in ESI) and that RGO forms a compact thin coating on PB deposit (Fig. S5din ESI). The voltammograms recorded in this case still reached a steady state response just after one voltammetric cycle and the shape of the voltammetric response was still characteristic of the

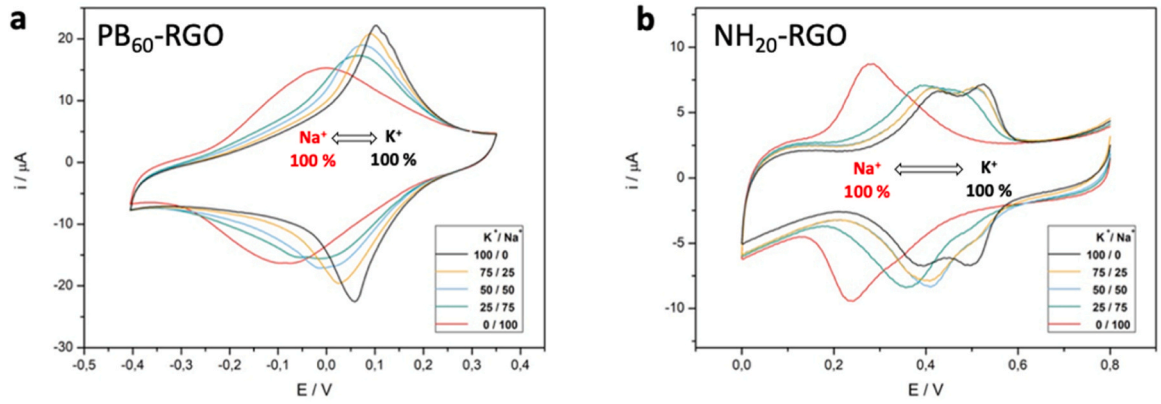

Fig. 3. CV responses obtained at (a) PB_{60}-RGO and (b) NH_{20}-RGO modified electrodes in acetate buffer solutions at different K^+/Na^+ ratio.

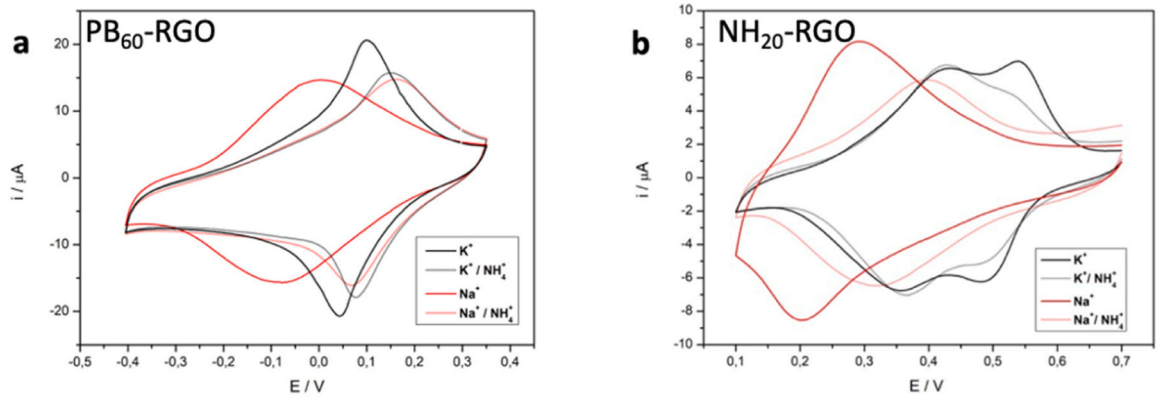

Fig. 4. CV responses recorded by (a) PB_{60}-RGO and (b) NH_{20}-RGO electrodes in 0.1 M of either K^+ (grey lines) or Na^+ (red lines), measured in presence of 0.1 M NH_4Cl (lightest lines) or without it (darker lines).

Na^+/K^+ ratio, however with a significant broadening of the K^+ peak (Fig. 3a and Fig. S1c). We attribute the broadening of K^+ peak to a lower diffusion of ions through RGO, which slowed down significantly the reduction process in presence of K^+.

Also NH electrodes were coated by a GO film, then reduced electrochemically to RGO. CV performed on such NH_{20}-RGO electrodes (Fig. 3b) in solutions containing K^+ showed a double peak corresponding to the electrochemical process of the $Fe(CN)_6^{4-/3-}$ redox couple. Such double peak is missing when only Na^+ is present. Moreover, the peaks shift at higher potentials at increasing the concentration of K^+, again due to the different intercalation of ions in NH, in agreement with previous results [22,47]. The responses obtained let us to conclude that also NH-RGO may be suitable for the quantification of Na^+ and K^+, as such or combined with PB-RGO electrodes.

3.2. Effect of interfering ions

We repeated the tests on K^+/Na^+ mixtures also in solutions including 0.1 M NH_4Cl, to mimic a more realistic system with the presence of an ion able to interfere significantly with the sensing mechanism since it can migrate into the crystalline structure of the inorganic complex during the electrochemical processes previously described.

Fig. 4 shows that the presence of NH_4Cl led to a significant shift of the PB reduction to less negative potentials. In particular, the peak, originally centered at −0.06 mV and 0.06 V in solutions only containing Na^+ and K^+, respectively, resulted nearly superimposed at *ca.* 0.1 V in solutions also containing NH_4^+. This is because NH_4^+ ions compete with K^+ and Na^+ to enter the PB lattice, minimizing the difference in the migration process originally present [18].

In case of NH electrodes in presence of NH_4^+ the differences associated to the oxidation process still remain, but are greatly reduced (Fig. 4b), with the peak observed in presence of Na^+ shifting from + 0.29 to + 0.40 V, much closer to the K^+ peak at + 0.43 V.

In presence of interfering NH_4Cl, thus, it would be difficult for a human eye to discriminate between superimposing CV curves; however, the trained ANN could still be able to discriminate the respective contributions of Na^+ and K^+ to the total curve by combining the information deriving from different kinds of sensors.

3.3. ANN elaboration

We thus used inputs from four types of sensors to define the concentration of K^+ and Na^+, i.e. PB and NH with two different thickness to further diversify the information given by the sensor platform, to exploit both the different intercalation mechanism in the two materials and the different diffusion in materials of different thickness. The resulting platform featuring multiple copies of the 4 electrodes was tested in all solutions reported in Table 1 following an experimental design for the collection of the dataset, then used to train the algorithm.

Before starting the training process by ANN, we randomized (or "shuffled") input dataframes. This step ensures that training, validation and test sets represent a fair sample of the data population [48]. Then, we split the dataset into the training (70 %), validation (20 %) and test (10 %) sets [38]. After that, we scaled the values of the training dataset, since it is an essential step in DL data pre-processing. To this aim, each data point A was scaled by a factor $<A>/\sigma$, where $<A>$ is the data mean and σ is the standard deviation [40].

Due to the size of the dataset, we used 8 Graphical Processing Units

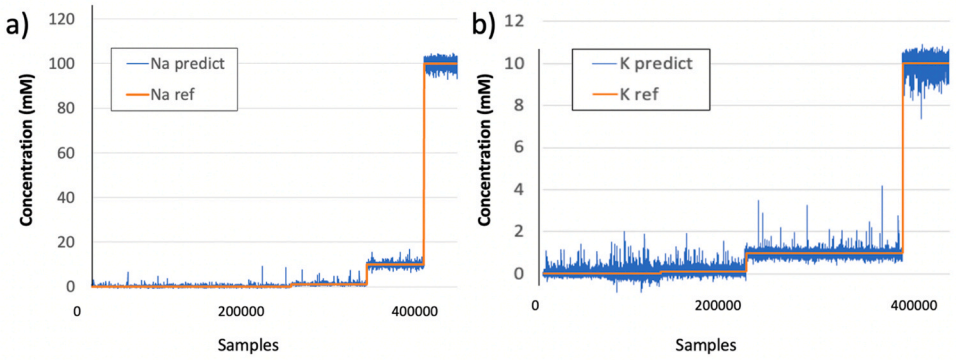

Fig. 5. Prediction test related to (a) [Na^+] and (b) [K^+] performed by the trained algorithm, comparing 10 % of dataset and the model obtained by 4 sensors with 300 epochs.

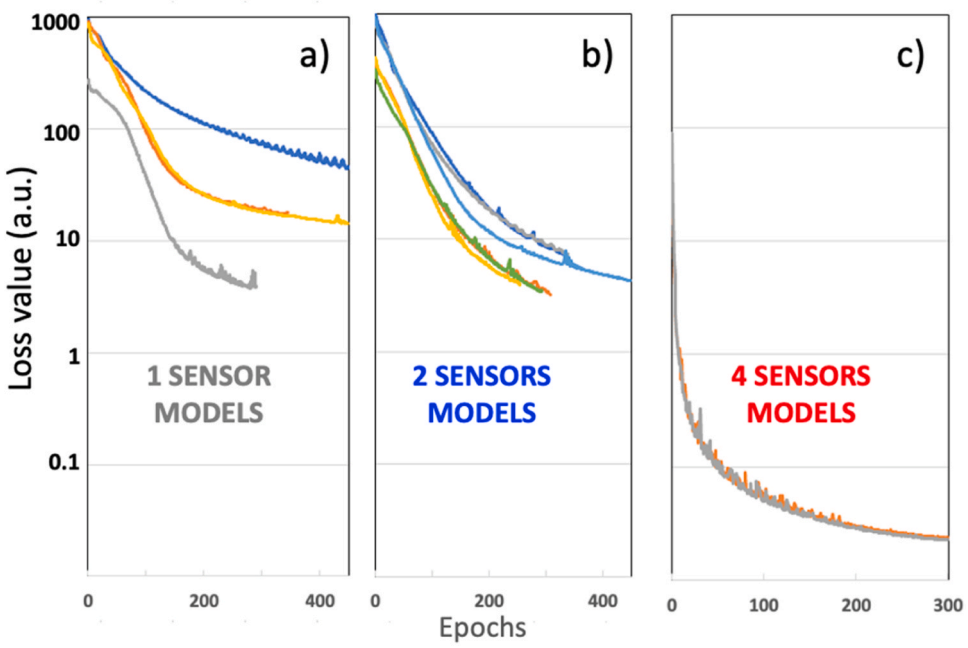

Fig. 6. Comparison of Validation Loss values across training of different models using: (a) only one sensor, (b) 2 sensors, or c) all four sensors. The Y scale is the same for all graphs. In (a), the sensor showing the best performance is the one using sensor PB_{60} (gray line), see main text.

(GPUs) in parallel to speed up the training process. We used the software libraries TensorFlow and Keras to define complex neural networks and build our DL model by defining some hyper parameters, such as the number of nodes per layer, the number of hidden layers and the batch size. Usually, input data are fed to the ANN in batches, i.e. portions of the whole training set, and the "batch size" defines how big this portion is. This allows to speed up the training process, especially when the input dataset is very large [48]. Other choices in model building include the loss functions, i.e. the error between the predicted and the true values, for each sample of the input dataset. The Learning Rate (LR) is another fundamental hyper-parameter since it directly controls the amount by which each weight increment is multiplied at every step of the algorithm. LR can be set to a constant value during training, or it can vary dynamically. We chose an exponential decaying LR defined as:

$$LR(s) = LR_0 \times d^{\left(\frac{s}{S}\right)} \quad (3)$$

Where LR_0 and d are the initial learning rate and decay rate ($d < 1$), s is the current step of the algorithm which depends on the current epoch and the current batch, and S is a scaling factor the number of steps. An exponential decaying LR follows a decreasing trend that allows to slow down the learning process as the number of epochs increases, in contrast with a constant LR. This allows to follow the slope (gradient) of the cost function (the curve that measures the error of the network across the entire dataset) more closely, having a faster learning when the curve is steeper (earlier epochs) and a slower learning when the curve is more gradual (later epochs) [39,48]. A constant LR, instead, may bring to learning steps that are too big in later epochs, thus not being able to follow the curve and resulting in an underfitting model (a sub-optimal solution to minimization of the cost function) [35,49].

The accuracy levels of the DL model defined was quite high: the predicted values are almost entirely in line with reference values for the concentration of both Na^+ (Fig. 5a) and K^+ (Fig. 5b).

We then checked if all different types of sensors are necessary to obtain a robust and accurate analysis. To this aim, we trained other models excluding on purpose one or more electrodes, to estimate the contribution of the different sensors to the final result. We compared the accuracy of models built for 4-sensors platform with simpler models based on only two or even just one sensor. Fig. 6 shows that the "multisensing" approach brings better accuracy in predictions: the validation loss (loss calculated on the validation set at each epoch end) obtained for models trained with data from a single sensor or from 2 sensors are two

Table 3
Comparison of best loss values obtained training the algorithm using one, two or all four sensors available. The sensors used in each case are reported in the columns on the right.

N. of sensors	Best loss Value	PB_{60}	PB_{120}	NH_{20}	NH_{50}
4	0.023	1	1	1	1
2	3.23	1		1	
2	3.43	1	1		
1	3.8	1			
2	3.88	1			1
2	4.28		1		1
2	7.31		1	1	
2	7.42			1	1
1	14.3		1		
1	17.6				1
1	44.5			1	

orders of magnitude higher than the one for the model with 4 sensors. Averaging on several training runs, the validation loss between real and predicted values for the model with 4 sensors was $2.3 \bullet 10^{-2}$, while the best value for models with 1 or 2 sensors was 3.23 (see Table 3). Moreover, the validation loss for models with 4 sensors converged faster than the one for models with 1 or 2 sensors (Fig. 6).

We also checked the importance of taking into account the cycle number *C* for the measurement (see Table 2), performing the training using the same data, with and without *C* column in the data array. Ignoring the cycle number led to ≈ 10 % increase of loss value, confirming that also the aging of the electrode has to be taken into account in such measurements.

4. Conclusions

The results obtained so far suggest that the detection voltammetric techniques can be combined with DL to have a good prediction of the concentration of Na^+ and K^+ ions in solution.

The advantage in the use of a voltammetric technique to predict the concentration of ions in solution is the linear dependence of the signal with respect to the concentration of analyte. The prediction of the concentration of Na^+ and K^+ by a voltammetric technique was only possible thanks to the use of DL approach, that allows to exploit all data acquired from the voltammetric results demonstrating that unoptimized sensors, working in parallel and in combination with a deep learning algorithm, could perform reliable measurements in realistic mixtures, on a broad range of concentrations. This could work even when the composition of the solutions was a challenging combination of analytes (as example, solution 1 in Table 1 contained 0.1 M NH_4^+, 10^{-4} M K^+ and no Na^+). The chemical affinity of the two ions targeted and the presence of an interfering ion rendered challenging even for somebody expert in the field to discriminate CV curves of the different solutions (see e.g. Fig. 3). However, the multivariate approach allowed to discriminate even tiny changes in the CV curves to measure the correct concentration. In our measurements, we did not try to optimize the selectivity or sensitivity of the materials used for the target analyte; for sure, the performance of such materials can be improved by tuning thickness, deposition methods, or even trying other combinations of 2D materials and 3D MOF, but this was outside the scope of this work. We do not claim that this could work with any solution containing Na^+, K^+ and NH_4^+, nor that it will work in real sweat or in presence of other interfering species. Improving such sensor arrays and testing them in different conditions is the subject of a different work; here, we focused on designing a suitable approach to use DL for electrochemical sensing in solutions.

We should underline that the main challenge in this approach is to produce massive amounts of coherent data needed to train the network; the production of these data requires to use multiple sensor arrays, fast measurements and sensor materials which need to be stable on long timescales. To partially address the issue of unpredictable changes in the sensing signal, we used as input of the network under training also the "age" of the electrode, in the form of the cycle number, which provided a ≈ 10 % significant benefit. The optimization of hyper-parameters (such as number of nodes, number of layers and finding an optimal learning rate) was also a fundamental part of the work.

A downside of using DL is that the final algorithm works as a "black box" providing the ion concentration, with no possibility to deduce chemical information on how the network combine the different sensor channels, and why.

To better understand the sensing performance, we trained different networks on the same data excluding different channels (Table 3). This tests provided some hint on which are the best performing materials for the sensing tasks. More refined methods shall also be used, as example principal component analysis (PCA) to reduce the dimensions of the dataset without losing relevant information; such technique has been already used for ML analysis of gas sensors, even if in that case only one single sensor type was used [50].

Overall, we believe that the approach demonstrated here could be applied also beyond the specific case of amperometric sensors, as example for tailored biological sensors or for light/radiation sensors, in every case where multiple sensors can be easily fabricated by tuning the material properties, sensor parameters or chemical functionalization.

CRediT authorship contribution statement

Vincenzo Palermo: Writing – review & editing, Writing – original draft, Supervision, Project administration, Funding acquisition, Conceptualization. **Lorenzo Tomasi:** Validation, Software, Methodology, Formal analysis. **Chiara Zanardi:** Writing – review & editing, Writing – original draft, Supervision, Project administration, Methodology, Conceptualization. **Giulia Cazzador:** Data curation. **Alessandro Kovtun:** Formal analysis. **Laura Malavolta:** Data curation. **Ilenia Bracaglia:** Data curation.

Declaration of Competing Interest

The authors declare that they have no known competing financial interests or personal relationships that could have appeared to influence the work reported in this paper.

Acknowledgements

The research leading to these results has received funding from the project *Deep-Sense*, funded by the Research Projects@CNR initiative.

Appendix A. Supporting information

Supplementary data associated with this article can be found in the online version at doi:10.1016/j.snb.2024.137194.

Data availability

Data will be made available on request.

References

[1] S. Anastasova, B. Crewther, P. Bembnowicz, V. Curto, H.M.D. Ip, B. Rosa, G. Z. Yang, A wearable multisensing patch for continuous sweat monitoring, Biosens. Bioelectron. 93 (2017) 139–145, https://doi.org/10.1016/j.bios.2016.09.038.
[2] M. Tessarolo, I. Gualaridi, B. Fraboni, Recent progress in wearable fully textile chemical sensors, Adv. Mater. Technol. 3 (2018) 1700310, https://doi.org/10.1002/admt.201700310.
[3] Y.R. Yang, W. Gao, Wearable and flexible electronics for continuous molecular monitoring, Chem. Soc. Rev. 48 (2019) 1465–1491, https://doi.org/10.1039/c7cs00730b.
[4] J.R. Sempionatto, I. Jeerapan, S. Krishnan, J. Wang, Wearable chemical sensors: emerging systems for on-body analytical chemistry, Anal. Chem. 92 (2020) 378–396, https://doi.org/10.1021/acs.analchem.9b04668.
[5] R. Colle, G. Grosso, A. Ronzani, M. Gazzano, V. Palermo, Anisotropic molecular packing of soluble C 60 fullerenes in hexagonal nanocrystals obtained by solvent vapor annealing, Carbon 50 (2012) 1332–1337, https://doi.org/10.1016/j.carbon.2011.11.003.
[6] H.C. Ates, P.Q. Nguyen, L. Gonzalez-Macia, E. Morales-Narváz, F. Guder, J. J. Collins, C. Dincer, End-to-end design of wearable sensors, Nat. Rev. Mater. 7 (2022) 887–907, https://doi.org/10.1038/s41578-022-00460-x.
[7] J.R. Sempionatto, J.A. Lasalde-Ramírez, K. Mahato, J. Wang, W. Gao, Wearable chemical sensors for biomarker discovery in the omics era, Nat. Rev. Chem. 6 (2022) 899–915, https://doi.org/10.1038/s41570-022-00439-w.
[8] H.Q. Zhang, R.Y. He, Y. Niu, F. Han, J. Li, X.W. Zhang, F. Xu, Graphene-enabled wearable sensors for healthcare monitoring, Biosens. Bioelectron. 197 (2022) 113777, https://doi.org/10.1016/j.bios.2021.113777.
[9] J.V. Vaghasiya, C.C. Mayorga-Martinez, M. Pumera, Wearable sensors for telehealth based on emerging materials and nanoarchitectonics, npj Flex. Electron. 7 (2023) 26, https://doi.org/10.1038/s41528-023-00261-4.
[10] F.P. Gao, C.X. Liu, L.C. Zhang, T.Z. Liu, Z. Wang, Z.X. Song, H.Y. Cai, Z. Fang, J. M. Chen, J.B. Wang, M.D. Han, J. Wang, K. Lin, R.Y. Wang, M.X. Li, Q. Mei, X. B. Ma, S.L. Liang, G.Y. Gou, N. Xue, Wearable and flexible electrochemical sensors for sweat analysis: a review, Microsyst. Nanoeng. 9 (1) (2023), https://doi.org/10.1038/s41378-022-00443-6.
[11] Z.F. Yin, Y. Yang, C. Hu, J.Z. Li, B.Y. Qin, X. Yang, Wearable respiratory sensors for health monitoring, NPG Asia Mater. 16 (2024) 8, https://doi.org/10.1038/s41427-023-00513-9.
[12] X.Q. Cui, Y. Bao, T.T. Han, Z.B. Liu, Y.M. Ma, Z.H. Sun, A wearable electrochemical sensor based on beta-CD functionalized graphene for pH and potassium ion analysis in sweat, Talanta 245 (2022) 123481, https://doi.org/10.1016/j.talanta.2022.123481.
[13] M. Parrilla, M. Cuartero, G.A. Crespo, Wearable potentiometric ion sensors, TrAC Trends Anal. Chem. 110 (2019) 303–320, https://doi.org/10.1016/j.trac.2018.11.024.
[14] J. Bobacka, A. Ivaska, A. Lewenstam, Potentiometric ion sensors, Chem. Rev. 108 (2008) 329–351, https://doi.org/10.1021/cr068100w.
[15] E. Bakker, V. Bhakthavatsalam, K.L. Gemene, Beyond potentiometry: robust electrochemical ion sensor concepts in view of remote chemical sensing, Talanta 75 (2008) 629–635, https://doi.org/10.1016/j.talanta.2007.10.021.
[16] G. Nagy, L. Nagy, Potentiometric Sensors, 2015. https://doi.org/10.1002/9781118684030.ch7.
[17] D. Ellis, M. Eckhoff, V.D. Neff, Electrochromism in the mixed-valence hexacyanides.1. Voltammetric and spectral studies of the oxidation and reduction of thin-films of prussian blue, J. Phys. Chem. 85 (1981) 1225–1231, https://doi.org/10.1021/j150609a026.
[18] P.J. Kulesza, S. Zamponi, M. Berrettoni, R. Marassi, M.A. Malik, Preparation, spectroscopic characterization and electrochemical charging of the sodium-containing analog of prussian-blue, Electrochim. Acta 40 (1995) 681–688, https://doi.org/10.1016/0013-4686(94)00348-5.
[19] A.A. Karyakin, Prussian Blue and its analogues: electrochemistry and analytical applications, Electroanalysis 13 (2001) 813–819, https://doi.org/10.1002/1521-4109(200106)13:10< 813::AID-ELAN813> 3.0.CO;2-Z.
[20] J.Q. Ang, B.T.T. Nguyen, Y. Huang, C.S. Toh, Ion-selective detection of non-intercalating Na^+ using competitive inhibition of K^+ intercalation in Prussian blue nanotubes sensor, Electrochim. Acta 55 (2010) 7903–7908, https://doi.org/10.1016/j.electacta.2010.04.025.
[21] Y. Matos-Peralta, M. Antuch, Review-Prussian Blue and its analogs as appealing materials for electrochemical sensing and biosensing, J. Electrochem. Soc. 167 (2019) 037510, https://doi.org/10.1149/2.0102003JES.
[22] J. Joseph, H. Gomathi, G.P. Rao, Electrochemical characteristics of thin-films of nickel hexacyanoferrate formed on carbon substrates, Electrochim. Acta 36 (1991) 1537–1541, https://doi.org/10.1016/0013-4686(91)85003-P.
[23] K. Itaya, T. Ataka, S. Toshima, Spectroelectrochemistry and electrochemical preparation method of prussian blue modified electrodes, J. Am. Chem. Soc. 104 (1982) 4767–4772, https://doi.org/10.1021/ja00382a006.
[24] H. Dussel, A. Dostal, F. Scholz, Hexacyanoferrate-based composite ion-sensitive electrodes for voltammetry, Fresenius J. Anal. Chem. 355 (1996) 21–28, https://doi.org/10.1007/s0021663550021.
[25] N. Bagkar, C.A. Betty, P.A. Hassan, K. Kahali, J.R. Bellare, J.V. Yakhmi, Self-assembled films of nickel hexacyanoferrate: electrochemical properties and application in potassium ion sensing, Thin Solid Films 497 (2006) 259–266, https://doi.org/10.1016/j.tsf.2005.11.002.
[26] J.R. Crespo-Rosa, G. Foca, A. Ulrici, L. Pigani, B. Zanfrognini, L. Cubillana-Aguilera, J.M. Palacios-Santander, C. Zanardi, Simultaneous detection of glucose and fructose in synthetic musts by multivariate analysis of silica-based amperometric sensor signals, Sensors 21 (2021) 4190, https://doi.org/10.3390/s21124190.
[27] B. Zanfrognini, A. Monari, G. Foca, A. Ulrici, L. Pigani, C. Zanardi, Preliminary evaluation of the use of a disposable electrochemical sensor for selective identification of 9-tetrahydrocannabinol and cannabidiol by multivariate analysis, Microchem. J. 183 (2022) 108108, https://doi.org/10.1016/j.microc.2022.108108.
[28] G. Foli, A. Kovtun, F. Liscio, E. Battaglini, S. Ligi, M. Fiorini, M. Minelli, V. Palermo, Tuneable permeability to H_2, CO_2, He, and Ar in graphene oxide−PDDA self-assembled multilayers, yielding good selectivity at high flux, Adv. Mater. Interfaces 11 (2024) 2300357–2300358, https://doi.org/10.1002/admi.202300357.
[29] L. Lancellotti, A. Bianchi, A. Kovtun, M. Gazzano, T.D. Marforio, Z. Xia, M. Calvaresi, M. Melucci, C. Zanardi, V. Palermo, Selective ion transport in large-area graphene oxide membrane filters, driven by ion radius and electrostatic interactions, Nanoscale 16 (2024) 7123, https://doi.org/10.1039/d3nr05874c.
[30] J.D. Qiu, J. Huang, R.P. Liang, Nanocomposite film based on graphene oxide for high performance flexible glucose biosensor, Sens. Actuators B Chem. 160 (2011) 287–294, https://doi.org/10.1016/j.snb.2011.07.049.
[31] N. Yusoff, A. Pandikumar, H.N. Ming, L.H. Ngee, Graphene-based electrochemical platform for biosensor applications, in: A. Tiwari, H.K. Patra, A.P.F. Turner (Eds.), Adv. Bioelectron. Mater., 2015: 187–214. https://doi.org/10.1002/9781118998861.
[32] S.K. Krishnan, E. Singh, P. Singh, M. Meyyappan, H.S. Nalwa, A review on graphene-based nanocomposites for electrochemical and fluorescent biosensors, RSC Adv. 9 (2019) 8778–8881, https://doi.org/10.1039/c8ra09577a.
[33] M. Coros, S. Pruneanu, R.I. Stefan-van Staden, Review-recent progress in the graphene-based electrochemical sensors and biosensors, J. Electrochem. Soc. 167 (2019) 037528, https://doi.org/10.1149/2.0282003JES.
[34] F. Poletti, B. Zanfrognini, L. Favaretto, V. Quintano, J. Sun, E. Treossi, M. Melucci, V. Palermo, C. Zanardi, Continuous capillary-flow sensing of glucose and lactate in sweat with an electrochemical sensor based on functionalized graphene oxide, Sens. Actuators B Chem. 344 (2021) 130253, https://doi.org/10.1016/j.snb.2021.130253.
[35] K. Sinha, Z. Uddin, H.I. Kawsar, S. Islam, M.J. Deen, M.M.R. Howlader, Analyzing chronic disease biomarkers using electrochemical sensors and artificial neural networks, TrAC Trends Anal. Chem. 158 (2023) 116861, https://doi.org/10.1016/j.trac.2022.116861.
[36] S. Dargan, M. Kumar, M.R. Ayyagari, G. Kumar, A survey of deep learning and its applications: a new paradigm to machine learning, Arch. Comput. Methods Eng. 27 (2020) 1071–1092, https://doi.org/10.1007/s11831-019-09344-w.
[37] F. Cui, Y. Yue, Y. Zhang, Z. Zhang, H.S. Zhou, Advancing biosensors with machine learning, ACS Sens 5 (2020) 3346–3364, https://doi.org/10.1021/acssensors.0c01424.
[38] I. Castiglioni, L. Rundo, M. Codari, G. Di Leo, C. Salvatore, M. Interlenghi, F. Gallivanone, A. Cozzi, N.C. D'Amico, F. Sardanelli, AI applications to medical images: From machine learning to deep learning, Phys. Med. 83 (2021) 9–24, https://doi.org/10.1016/j.ejmp.2021.02.006.
[39] L. Yang, A. Shami, On hyperparameter optimization of machine learning algorithms: theory and practice, Neurocomputing 415 (2020) 295–316, https://doi.org/10.1016/j.neucom.2020.07.061.
[40] S. Theodoridis, Machine learning. A Bayesian and Optimization Perspective, Academic Press, 2015, https://doi.org/10.1016/C2019-0-03772-7.
[41] S. Namuduri, B.N. Narayanan, V.S.P. Davuluru, L. Burton, S. Bhansali, Review-deep learning methods for sensor based predictive maintenance and future perspectives for electrochemical sensors, J. Electrochem. Soc. 167 (2020) 037552, https://doi.org/10.1149/1945-7111/ab67a8.
[42] M. Luca, G. Barlacchi, B. Lepri, L. Pappalardo, A survey on deep learning for human mobility, ACM Comput. Surv. 55 (2023) 1–44, https://doi.org/10.1145/3485125.
[43] S. Lupu, C. Mihailciuc, L. Pigani, R. Seeber, N. Totir, C. Zanardi, Electrochemical preparation and characterisation of bilayer films composed by Prussian Blue and conducting polymer, Electrochem. Commun. 4 (2002) 753–758, https://doi.org/10.1016/S1388-2481(02)00440-X.
[44] Z.Y. Xia, M. Christian, C. Arbizzani, V. Morandi, M. Gazzano, V. Quintano, A. Kovtun, V. Palermo, A robust, modular approach to produce graphene-MOx

multilayer foams as electrodes for Li-ion batteries, Nanoscale 11 (2019) 5265–5273, https://doi.org/10.1039/c8nr09195a.
[45] F. Perrozzi, S. Prezioso, M. Donarelli, F. Bisti, P. De Marco, S. Santucci, M. Nardone, E. Treossi, V. Palermo, L. Ottaviano, Use of optical contrast to estimate the degree of reduction of graphene oxide, J. Phys. Chem. C 117 (2013) 620–625, https://doi.org/10.1021/jp3069738.
[46] G. Maccaferri, C. Zanardi, Z.Y. Xia, A. Kovtun, A. Liscio, F. Terzi, V. Palermo, R. Seeber, Systematic study of the correlation between surface chemistry, conductivity and electrocatalytic properties of graphene oxide nanosheets, Carbon 120 (2017) 165–175, https://doi.org/10.1016/j.carbon.2017.05.030.
[47] S. Zamponi, M. Berrettoni, P.J. Kulesza, K. Miecznikowski, M.A. Malik, O. Makowski, R. Marassi, Influence of experimental conditions on electrochemical behavior of Prussian blue type nickel hexacyanoferrate film, Electrochim. Acta 48 (2003) 4261–4269, https://doi.org/10.1016/j.electacta.2003.08.001.
[48] I. Goodfellow, Y. Bengio, A. Courville, I. Goodfellow, Y. Bengio, A. Courville, Deep Learning, in: Deep Learning (2016) 1–775.
[49] R.Y. Choi, A.S. Coyner, J. Kalpathy-Cramer, M.F. Chiang, J.P. Campbell, Introduction to machine learning, neural networks, and deep learning, Transl. Vis. Sci. Technol. 9 (2020) 14, https://doi.org/10.1167/tvst.9.2.14.
[50] S. Huang, A. Croy, L.A. Panes-Ruiz, V. Khavrus, V. Bezugly, B. Ibarlucea, G. Cuniberti, Machine learning-enabled smart gas sensing platform for identification of industrial gases, Adv. Intel. Syst. 4 (2022) 2200016, https://doi.org/10.1002/aisy.202200016.

Laura Malavolta obtained her Master's degree cum laude in Materials Engineering and Nanotechnology at Politecnico di Milano, with thesis "Electrochemical behavior of anodic materials for bioelectrochemical systems". She obtained her Bachelor's degree in Chemical and Biochemical Engineering - stage and thesis in Electrochemistry "Studio di separatori modificati per batterie al litio" (Study on modified separators for lithium batteries).

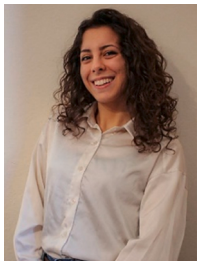

Ilenia Bracaglia is a Ph.D. student at the University of La Sapienza in Rome. Her master's thesis focused on analytical forensic chemistry, particularly involving illicit drugs. She developed UPLC-MS/MS methods for detecting drugs in various matrices, collaborating with law enforcement. She later worked as a research fellow at the CNR Institute, applying machine learning to electrochemical biosensor data for diagnosing biomedical conditions. Currently, she is expanding her expertise in data processing, using multivariate methods to address the issue of New Psychoactive Substances in Italy, supporting forensic and toxicology fields.

Giulia Cazzador is a Ph.D. Student in Science and Technology of Bio and Nanomaterials at Ca' Foscari University of Venice, Italy. She works in Nano@Sense Group under the supervision of Prof. Chiara Zanardi. Her Ph.D. research regards the development of wearable sensors for the detection of biomarkers in sweat. She obtained the master's degree in chemistry at the Department of Molecular Science and Nanosystem (DSMN) of the Ca' Foscari University of Venice.

Alessandro Kovtun is a permanent researcher at the Institute for Organic Synthesis and Photoreactivity (ISOF) of the Italian National Research Council (CNR) in Bologna, Italy. His expertise lies in spectroscopy data analysis, particularly in X-ray Photoelectron Spectroscopy, Raman, and Energy-Dispersive X-ray Spectroscopy, as well as Scanning Electron Microscopy (SEM). He focuses on the chemical functionalization, adsorption properties, and transport phenomena of 2D materials, with a particular emphasis on graphene, graphene oxide, and reduced graphene oxide.

Lorenzo Tomasi is a technologist at CNR Institute for Organic Synthesis and Photoreactivity (ISOF) in Italy. He is a computer scientist with more than 20 years of experience as a software developer and system administrator. Before working at CNR, he worked in other public research institutions in Italy such as ENEA and CINECA. He started his work in ISOF by contributing to a research project about smart cities in 2015. During this project, he used artificial intelligence to analyse data from environmental sensors. More recently, he also used AI to analyse data from neural cells signals recording. During his career at ISOF, he contributed to several research projects as a data scientist and artificial intelligence algorithms developer.

Chiara Zanardi is Full Professor of Analytical Chemistry at the Department of Molecular Sciences and Nanosystems of the Ca' Foscari University of Venice and associated to the Institute for Organic Synthesis and Photoreactivity (ISOF) of CNR in Bologna. She graduated in Industrial Chemistry at the University of Bologna and she obtained the Ph.D. in Chemical Sciences from the University of Modena and Reggio Emilia. Her expertise mainly concerns the development of modified electrodes and their application as amperometric sensors for the monitoring of human health, environmental pollutants and foodstuffs safety. She is the head of the Nano@Sens group, a research team specifically aimed at the application of nano-sized materials to the realization of electrochemical sensors for water pollutants and biomarkers in biological fluids. She is the co-author of more that 100 papers printed on peer-review journals, two patents, one book and three book chapters dealing with modified electrodes in electroanalysis.

Vincenzo Palermo is the director of the CNR Institute for Organic Synthesis and Photoreactivity (ISOF) in Bologna, Italy, and associated professor of Chalmers University of Technology (Sweden). He uses nanotechnology and supramolecular chemistry to create new materials for electronics, aerospace and biomedical applications. He published > 210 scientific articles on international journals in chemistry, nanotechnology and materials science (>12 000 citations, h-index 55), collaborating with key industrial partners in Europe (Airbus, FCA, Leonardo, BASF, Nokia, STMicroelectronics etc.). He coordinated several EU projects in the past, including being vice-director and member of the executive board of the Graphene Flagship, one of the largest research projects ever launched in Europe. He has been awarded the Lecturer Award for Excellence of the Federation of European Materials Societies (FEMS), the Research Award of the Italian Society of Chemistry (SCI) and the Science dissemination awards of the Italian Book Association.